

Polycyclic aromatic hydrocarbons in spatially resolved extragalactic star forming complexes

M. S. Khramtsova^{1*}, D. S. Wiebe¹, P. A. Boley², Ya. N. Pavlyuchenkov¹

¹Institute of Astronomy, Russian Academy of Sciences, Pyatnitskaya str. 48, Moscow 119017, Russia

²Max Planck Institute for Astronomy, Königstuhl 17, Heidelberg D69117, Germany

1 November 2021

ABSTRACT

The abundance of polycyclic aromatic hydrocarbons (PAHs) in low- and high-metallicity galaxies has been widely discussed since the time when detailed infrared data for extragalactic objects were first obtained. On the scales of entire galaxies, a smaller PAH abundance in lower-metallicity galaxies is often observed. We study this relationship for star-forming regions in nearby galaxies, for a sample containing more than 200 HII complexes, using spatially-resolved observations from the Herschel Space Observatory and Spitzer Space Telescope. We use a model for the dust emission to estimate the physical parameters (PAH abundance, metallicity, ultraviolet radiation field, etc.) of these complexes. The same correlation of PAH abundance with metallicity, as seen for entire galaxies, is apparently preserved at smaller scales, at least when the Kobulnicky & Kewley metallicity calibration is used. We discuss possible reasons for this correlation, noting that traces of less-effective PAH formation in low-metallicity AGB stars should be smeared out by radial mixing in galactic disks. Effective destruction by the harder and more intensive ultraviolet field in low-metallicity environments is qualitatively consistent with our data, as the ultraviolet field intensity, derived from the infrared photometry, is indeed smaller in HII complexes with lower metallicity.

Key words: infrared: galaxies – ISM, galaxies: photometry

1 INTRODUCTION

Polycyclic aromatic hydrocarbons (PAHs) are now a well-recognized component of the interstellar medium (ISM), both in our Galaxy, and in external galaxies. Along with very small grains (VSGs, $r \sim 100$ Å), PAHs are believed to be the dominant source of non-stellar emission in the near-infrared and mid-infrared ranges ($2 - 20$ μm) in star-forming galaxies. This emission often constitutes a sizable fraction of a galaxy's total infrared luminosity (Smith et al. 2007), and cannot be explained by large grains alone, which are too cold in the diffuse ISM to emit at these wavelengths. On the other hand, grains with radii much smaller than the typically-assumed value of 0.1 μm can heat up to very high temperatures upon a single photon absorption. Thus, stochastically-heated VSGs can produce mid-infrared continuum emission, while radiatively-excited bending and vibrational modes in PAHs are the source of several spectral features in the $\sim 2 - 20$ μm wavelength range.

As an ultraviolet (UV) photon is needed to excite a PAH or VSG particle, the emission from these particles should be related to the overall UV emission (Draine & Li

2001; Li & Draine 2002). Because of this expected connection between the UV luminosity and the infrared (IR) luminosity, specific PAH bands, mid-IR continuum, and their combinations with other observables are now considered as possible indicators of star formation (e.g., Calzetti et al. 2007; Zhu et al. 2008; Kennicutt et al. 2009; Treyer et al. 2010; Kim et al. 2012). However, the UV radiation that excites PAH molecules can also destroy these particles, depending on the strength and hardness of the radiation field. The harsher UV fields expected in star-forming regions can therefore cause a significant local depletion of small particles; thus, the relation between PAH emission and the star formation rate (SFR) can be more complicated than a simple monotonic function. To assess the applicability of PAH emission as a tracer of the SFR, it is necessary to consider processes of both their formation and destruction in detail.

Despite the significant observational progress in this field, some key theoretical questions about the PAH lifecycle are still debated. Of particular interest, both for PAH physics and for their usage as a SFR indicator, is the empirically-derived relation between the metallicity of a galaxy and the relative PAH abundance (Engelbracht et al. 2005; Madden et al. 2006; Draine et al. 2007; Smith et al. 2007; Wu et al. 2007; Hunt et al. 2010). Specifically, there

* E-mail: khramtsova@inasan.ru

appears to exist a metallicity threshold ($12 + \log(\text{O}/\text{H})$ from ≈ 8.0 to 8.4 (depending on the adopted metallicity calibration) which separates galaxies into groups with high and low PAH abundance (in terms of the PAH fraction of the total dust mass, i.e. q_{PAH}).

Two general scenarios has been proposed to explain the origin of this threshold. If PAHs are synthesized in the atmospheres of carbon-rich asymptotic giant branch (AGB) stars (Latter 1991), the efficiency of their production should depend on the carbon-to-oxygen ratio, which can be a function of metallicity. According to this scenario, PAHs are formed less efficiently by evolved stars in low-metallicity galaxies (Galliano et al. 2008). According to the “destructive” scenario, PAH destruction can be more intensive in low-metallicity environments due to the harder UV-field (Galliano et al. 2005; Madden et al. 2006) or stronger shocks (O’Halloran et al. 2006). As neither of these scenarios now seems clearly preferable, the question of the formation and destruction of large molecules in these environments requires additional study.

Studies of PAHs have been tightly related to the development of infrared telescopes. Our knowledge about their presence and importance has expanded significantly, thanks to the Infrared Space Observatory (ISO) and especially to the Spitzer Space Telescope. The Spitzer IRAC and MIPS passbands cover PAH spectral features, in addition to continuum emission from larger grains. The combination of observations at short ($3.6 - 24 \mu\text{m}$) and long (70 and $160 \mu\text{m}$) wavelengths makes it possible to determine the PAH abundance relative to the total dust mass in extragalactic objects (Draine & Li 2007). However, for many galaxies, only unresolved photometry can be performed with Spitzer at longer wavelengths, where the spatial resolution ($\sim 38''$) is not sufficient to measure individual fluxes from smaller regions. It is thus not possible to resolve individual HII regions and star-forming complexes at these wavelengths in most galaxies, except the for Large and Small Magellanic Clouds (e.g., Slater et al. 2011; Sandstrom et al. 2010, correspondingly), M101 (Gordon et al. 2008), and some others (e.g., Haynes et al. 2010).

Muñoz-Mateos et al. (2009) performed a spatially resolved study of the dust properties of galaxies in the SINGS sample (Kennicutt et al. 2003) on a scale larger than that of individual HII complexes, using azimuthally-averaged emission profiles. They found that the correlation between the metallicity and PAH content is observed not only in a galaxy as a whole, but also radially. They conclude that at large spatial scales this correlation is more readily explained by evolutionary effects. In that work, no distinction is made between PAHs in star-forming regions and PAHs in the general diffuse ISM.

We can expect that the details of PAH physics will be revealed with more clarity in spatially-resolved observations of individual star-forming regions and complexes, rich in bright UV-sources, both heating PAHs and destroying them. The intensity of $8 \mu\text{m}$ emission, and its correlation with metallicity, may depend on the source of heating. Within (or close to) HII regions, PAHs are heated by single ultraviolet photons produced by young stars. However, at some distance from these regions, the radiation field from older stellar populations can heat PAHs as well, and their emission is thus no longer a direct SFR tracer (Boselli et al.

2004; Bendo et al. 2008; Crocker et al. 2013). Therefore, it is desirable to separately observe PAH emission both in the vicinity of HII complexes, and in the general diffuse interstellar medium.

To achieve this goal, we need the ability to study individual star-forming regions and complexes, both at the mid- and far-IR wavelengths. The resolution at 70 and $160 \mu\text{m}$ provided by the Herschel Space Observatory (about $5.2''$ and $12''$, respectively) partly satisfies the requirements. Corresponding physical scale is about several hundred parsecs for nearby galaxies. This resolution in most cases does not allow studying individual HII regions but is sufficient to analyse large HII complexes and filaments. Thus, the Herschel data successfully complement the Spitzer data at shorter wavelengths, which have a resolution of less than $1-2''$ for IRAC the passbands ($3.6-8.0 \mu\text{m}$), and $\sim 7''$ for MIPS $24 \mu\text{m}$.

Previously, the spatially resolved analysis of the mid-IR properties and their relation to the metallicity was performed by Gordon et al. (2008) for a large sample of HII regions in M101. The goal of this paper is to extend this sample significantly and to study the properties of PAH emission in individual HII complexes within several nearby galaxies at various metallicities, using data from the Spitzer and Herschel telescopes. We consider possible correlations between the various derived properties of the HII complexes, and discuss the main scenarios for PAH formation and destruction in the context of these observations.

2 OBSERVATIONAL DATA

For this work, we consider 24 galaxies which were observed with both the Spitzer Space Telescope and the Herschel Space Observatory. All of the Spitzer data examined in this paper were observed as part of the SINGS survey (Kennicutt et al. 2003), and most of the Herschel data were observed as part of the KINGFISH survey (Kennicutt et al. 2011), although we also include data for 3 galaxies (NGC 2403, NGC 6822, NGC 5194) which were observed with Herschel as parts of other programs. In Table 1, we list the name and morphological type of each galaxy (from Moustakas et al. 2010), together with the proposal identification number (Prop. ID) and principal investigator for the Herschel data presented here. We also list the number of HII complexes, analysed in each galaxy, and references to the works used to identify them. In the last column we indicate the physical resolution for each galaxy probed by the Herschel instruments. For most galaxies, the resolution is about a few hundred parsec, however, in some cases it is about 200 pc or even less which could mean that we probe individual giant HII regions.

For the galaxies in Table 1, we consider only data obtained with the IRAC and PACS (Poglitsch et al. 2010) instruments on Spitzer and Herschel, respectively. We downloaded the reduced IRAC images at wavelengths of 3.6 , 4.5 , 5.8 and $8.0 \mu\text{m}$ from the SINGS project website¹. For the Herschel data, we consider images at 70 and $160 \mu\text{m}$, obtained with the PACS photometer. We downloaded the so-called Level 1 data from the Herschel Science Archive²,

¹ <http://sings.stsci.edu>

² http://herchel.esac.esa.int/Science_Archive.shtml

which were reduced with version 6.1.1 of the automated reduction pipeline. We produced final maps from the Level 1 data using version 16 of the Scanamorphos algorithm (Roussel 2012), with a pixel scale of $2''.0$.

3 METHODS OF MEASUREMENTS AND ANALYSIS

3.1 Photometry

Since the point spread functions (PSFs) of the observations from different instruments and passbands differ from each other, we convolved all shorter-wavelength images to the resolution of $160 \mu\text{m}$ PACS images, using the IDL convolution procedure and kernels provided by Aniano et al. (2011). Finally, all the images were resampled to have a pixel scale of $2''.0$.

The convolved and resampled images were used to perform aperture photometry in the following fashion: the flux in an aperture is measured for each HII complex for which the metallicity is available in the work by Moustakas et al. (2010). The aperture radius is chosen separately for each HII complex, depending on its size, but they are not less than the size of the lowest resolution element ($12''$). Therefore, no aperture corrections were applied. The centre of an aperture is chosen geometrically. Finally, we correct the flux for the contribution of partial pixels.

To subtract the background emission, we estimate its average value and standard deviation, σ_{ring} , within a ring having a width of a few arcseconds around the aperture. To exclude bright sources (e.g., neighbouring HII complexes) from the ring, we take into account only pixels with intensities smaller than $3\sigma_{\text{ring}}$. As the shift of an aperture by 1 pixel may significantly (by $\sim 10\%$) change the estimated background, we move the centre of each aperture in all directions by 1 pixel (in steps of 0.5 pixel) and calculate the average flux for all aperture positions. This reduces the influence of the position error, too. The standard deviation from this average is σ_{pos} . The two uncertainties, σ_{pos} and σ_{ring} , are comparable in magnitude and in most cases contribute more or less equally to the total uncertainty. The final error of the aperture flux, σ , is then equal to

$$\sigma = \sqrt{\sigma_{\text{ring}}^2 + \sigma_{\text{pos}}^2}. \quad (1)$$

This value varies from 1% to 10% for most complexes, but can be larger for faint complexes that cannot be clearly separated from neighbouring complexes. Locations with a signal-to-noise ratio < 3 at $8 \mu\text{m}$ are excluded from the study, which means that only large and bright complexes are analysed, as small and faint complexes are discarded because of the convolution process. The results of photometry for all bands are presented in Table 2 (see below).

Finally, we note that measuring reliable fluxes for low-metallicity galaxies, like DDO 053 and Holmberg I, is complicated by the extremely low signal-to-noise ratio. As a result, we had to abandon most complexes from these galaxies, but we present fluxes for some of the brighter complexes in Table 2 (see below).

3.2 Fitting HII Complex Spectra

We apply the algorithm that has been used in Draine et al.

(2007) to calculate global SEDs of SINGS galaxies, but use it to compute emission spectra of individual HII complexes. To model a dust emission spectrum, we adopt the Draine & Li (2007) approach but use an alternative method of computing temperature distribution functions. Details are provided below.

We assume that a theoretical emission spectrum of an HII complex, located at the distance D , is given by (Draine et al. 2007)

$$f_{\nu, \text{model}} = \Omega_{\star} B_{\nu}(T_{\star}) + \frac{M_{\text{dust}}}{4\pi D^2} \left[(1 - \gamma) p_{\nu}^0(q_{\text{PAH}}, U_{\text{min}}) + \gamma p_{\nu}^1(q_{\text{PAH}}, U_{\text{min}}) \right]. \quad (2)$$

Here the first term with $T_{\star} = 5000 \text{ K}$ describes the stellar contribution, M_{dust} is the total dust mass in the HII complex and Ω_{\star} is the starlight dilution parameter.

The radiation field in a complex is described by the scaling factor U , which is given in units of the interstellar radiation field u_{ν}^0 in the solar vicinity, as estimated by Mathis et al. (1983). Thus, the energy density of the radiation field u_{ν} is $U \times u_{\nu}^0$. For U , we use the representation given by Eq. 23 from Draine & Li (2007). In this representation, a fraction $1 - \gamma$ of all the dust is exposed to the “minimum” radiation field U_{min} , while the remaining dust is illuminated by the enhanced radiation field, having a power-law distribution with an exponent of α , and an upper limit of U_{max} . As in Draine et al. (2007), we adopt the fixed values $U_{\text{max}} = 10^6$ and $\alpha = 2$. Functions p_{ν}^0 and p_{ν}^1 represent emission per unit frequency per unit mass of dust (with a PAH fraction q_{PAH}) illuminated by the minimum radiation field and by the enhanced radiation field, respectively.

We adopt a grain model from Draine & Li (2007) which represents a dust mixture consisting of carbonaceous particles (including VSGs and PAHs) and amorphous silicates. The Milky Way dust with $R_{\text{V}} = 3.1$ is utilized. For grains larger than 250 \AA an equilibrium temperature is calculated for a given starlight intensity. For smaller grains we take the stochastic heating into account and calculate the temperature distribution functions as described by Pavlyuchenkov et al. (2012).

We follow the fitting procedure described in Draine et al. (2007). The best-fit SED for an HII complex is found using the observed fluxes at 3.6, 4.5, 5.8, 8.0, 24, 70, and $160 \mu\text{m}$. The fitting parameters are the PAH mass fraction q_{PAH} , the minimum starlight intensity U_{min} , the parameter γ describing the fraction of dust heated by radiation field with intensity greater than U_{min} , the dust mass M_{dust} and the solid angle Ω_{\star} of stellar emission. The last two parameters are used for normalization only.

In the parameter grid, used for fitting, the q_{PAH} values range from 0.47 to 4.6% (a step is 0.1); the minimum starlight U_{min} varies from 0.1 to 25 (a step is 0.1); and γ varies from 0 to 0.3 (we sample this parameter 10 times within this range in logarithmic scale). The best-fit model is the model with the minimum value of χ^2 , where χ^2 is given by

$$\chi^2 = \sum_{\text{band}} \frac{(f_{\nu, \text{band}}^{\text{obs}} - f_{\nu, \text{band}}^{\text{model}})^2}{(\sigma_{\text{band}}^{\text{obs}})^2 + (\sigma_{\text{band}}^{\text{model}})^2}. \quad (3)$$

Here $f_{\nu, \text{band}}^{\text{obs}}$ and $\sigma_{\text{band}}^{\text{obs}}$ are the observed flux density at a given passband and the uncertainty of this value, while

Table 1. Sample of galaxies

Object	Prop. ID	Proposer	Type	Number of complexes	Ref.	Physical resolution, kpc
DDO 53	KPOT_rkennicu_1	R. Kennicutt	Im	2	5	0.21
Holmberg I	KPOT_rkennicu_1	R. Kennicutt	IABm	1	5	0.22
Holmberg II	KPOT_rkennicu_1	R. Kennicutt	Im	6	20	0.20
IC 2574	KPOT_rkennicu_1	R. Kennicutt	SABm	7	5,21	0.23
NGC 628	KPOT_rkennicu_1	R. Kennicutt	SAC	11	1,2,3,4	0.42
NGC 925	KPOT_rkennicu_1	R. Kennicutt	SABd	23	2	0.53
NGC 1097	SDP_rkennicu_3	R. Kennicutt	SBb	6	6	0.99
NGC 2403	KPGT_cwilso01_1	C. Wilson	SABcd	11	7,8	0.18
NGC 3184	KPOT_rkennicu_1	R. Kennicutt	SABcd	14	2,9	0.65
NGC 3198	KPOT_rkennicu_1	R. Kennicutt	SBc	8	9	0.80
NGC 3351	KPOT_rkennicu_1	R. Kennicutt	SBb	6	1,15	0.54
NGC 3521	KPOT_rkennicu_1	R. Kennicutt	SABbc	8	1,9	0.58
NGC 3621	KPOT_rkennicu_1	R. Kennicutt	SAd	21	9,16	0.38
NGC 4254	KPOT_rkennicu_1	R. Kennicutt	SAC	10	3,17,18	0.96
NGC 4321	KPOT_rkennicu_1	R. Kennicutt	SABbc	7	3,18	0.83
NGC 4559	SDP_rkennicu_3	R. Kennicutt	SABcd	12	9	0.60
NGC 4725	KPOT_rkennicu_1	R. Kennicutt	SABab pec	7	9	0.69
NGC 4736	KPOT_rkennicu_1	R. Kennicutt	SAab	7	1,14	0.30
NGC 5055	KPOT_rkennicu_1	R. Kennicutt	SAbc	5	3	0.45
NGC 5194	KPGT_cwilso01_1	C. Wilson	SABbc pec	14	10,11	0.44
NGC 6822	SDP_smadde01_3	S. Madden	IBm	5	12,13	0.02
NGC 6946	KPOT_rkennicu_1	R. Kennicutt	SABcd	7	3,4	0.40
NGC 7331	KPOT_rkennicu_1	R. Kennicutt	SAb	2	1,14	0.84
NGC 7793	KPOT_rkennicu_1	R. Kennicutt	SAd	9	3,19	0.23

References: (1) Bresolin et al. (1999), (2) van Zee et al. (1998), (3) McCall et al. (1985), (4) Ferguson et al. (1998), (5) Croxall et al. (2009), (6) Lee & Skillman (2004), (7) Garnett et al. (1999), (8) Garnett et al. (1997), (9) Zaritsky et al. (1994), (10) Bresolin et al. (2004), (11) Diaz et al. (1991), (12) Lee et al. (2006), (13) Hodge et al. (1988), (14) Oey & Kennicutt (1993), (15) Bresolin & Kennicutt (2002), (16) Ryder (1995), (17) Henry et al. (1994), (18) Shields (1991), (19) Edmunds & Pagel (1984), (20) Hodge et al. (1994), (21) Arsenault & Roy (1986)

$f_{\nu, \text{band}}^{\text{model}}$ and $\sigma_{\text{band}}^{\text{model}}$ are the theoretical flux density and its “uncertainty,” which has been proposed by Draine et al. (2007) to account for different levels of uncertainties in different bands. It is estimated as $0.1 f_{\nu, \text{band}}^{\text{model}}$. The best-fit χ^2 values vary from 0.5 to 3, depending on the region. Uncertainties in the derived parameters are calculated using the Monte-Carlo method.

3.3 Metallicities of the HII complexes

Many different methods have been developed to determine the metallicity of HII regions. One of the main methods is the so-called “direct” T_e method, based on the electron temperature measurement (e.g. Stasińska 2007). However, this method requires observations of very faint nebular lines, and consequently is of limited use. Besides this, various other “indirect” methods can be used. While numerous methods are available, metallicity estimates obtained with different methods may differ significantly (up to 0.7 dex). Thus, regardless of which particular method is chosen, it is important for consistency to use the same method to evaluate the metallicities for all HII regions.

We use the metallicities of HII complexes in the SINGS galaxies calculated by Moustakas et al. (2010). They collected spectroscopic data from various sources and used two methods to estimate metallicities. These methods are the theoretical relationship presented by Kobulnicky & Kewley (2004) (hereafter, KK04) and the empirically-derived rela-

tionship of Pilyugin & Thuan (2005) (hereafter, PT05). In both methods, relatively strong nebular lines ([O ii] λ 3727; [O iii] λ 4959, 5007; H β) are utilized.

These methods are convenient for a number of reasons. First, estimates obtained with them tend to bracket metallicities determined by various other methods. In other words, the “true” value of metallicity presumably lies somewhere within the range bounded by values calculated with the KK04 and PT05 methods. Second, while other indirect methods are recommended for objects with specific values of luminosity, metallicity, etc., the KK04 and PT05 methods are more or less universal. The HII complexes in our sample possess a wide range of physical properties, so this “universality” is desirable. For further discussions and a comparison of these methods, we refer to the publication by Moustakas et al. (2010), but some points are worth to be repeated here.

First, metallicities determined with the KK04 method are systematically higher than those determined with the PT05 method (Fig. 1). As the latter metallicities are similar to metallicities obtained with the T_e method (Egorov et al. 2012), the KK04 method results are also systematically higher than “direct” metallicity estimates. Second, when the PT05 metallicities are plotted versus galactocentric radius, they show shallower gradients and much more scatter than the KK04 metallicities (Moustakas et al. 2010). We see the scatter in our results, too (see below). Furthermore, López-Sánchez et al. (2012) compared these methods, and

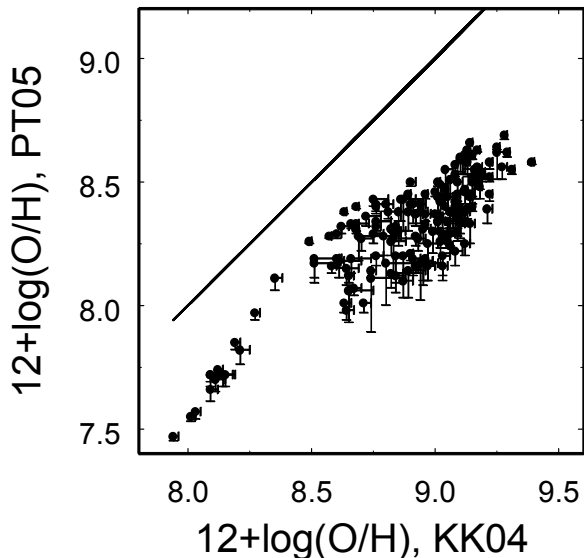


Figure 1. Comparison of metallicities estimated by KK04 and PT05 methods. A straight line $y = x$ is added for clarity.

suggested that the KK04 method produces the most reliable metallicities for stellar populations.

4 RESULTS

The results of the aperture photometry are presented in Table 2, with the following columns: (1) sequential number; (2) designation of the HII complex; (3)-(4) right ascension and declination of the complex; (5) an aperture size; and (6)-(12) the fluxes at IRAC 3.6, 4.5, 5.8, 8.0, MIPS 24, PACS 70, and PACS 160 μm bands. The results of fitting procedure are presented in Table 3, which contains the following columns: (1) sequential number; (2) designation; (3) the relative PAH mass abundance, q_{PAH} ; (4) γ parameter; (5) minimum starlight intensity U_{min} ; (6) and (7) metallicities of the complex, determined by Moustakas et al. (2010) with the KK04 and PT05 methods.

The values of q_{PAH} , γ and U_{min} have been determined for each galaxy in the SINGS sample by Draine et al. (2007). In Fig. 2, we compare the values of q_{PAH} and U_{min} for each galaxy, obtained by simple averaging of the values from Table 3, with the respective values given by Draine et al. (2007). Note that in Draine et al. (2007) the parameters were obtained based on global photometry of galaxies including diffuse medium not associated with HII complexes which can contribute a significant fraction to the total infrared emission. The PAH abundances in both studies agree well with each other, while our starlight intensities are systematically higher than the values of Draine et al. (2007) (the same is true for γ as well). This is expected, as we only consider HII complexes, and our U_{min} starlight intensities are biased toward higher values.

Since we are mostly interested in PAHs, below we consider several relations between the metallicity and parameters related to PAHs. Note that complexes with minimum and maximum q_{PAH} values represent, correspondingly, upper and lower limits. In this study we use the models for

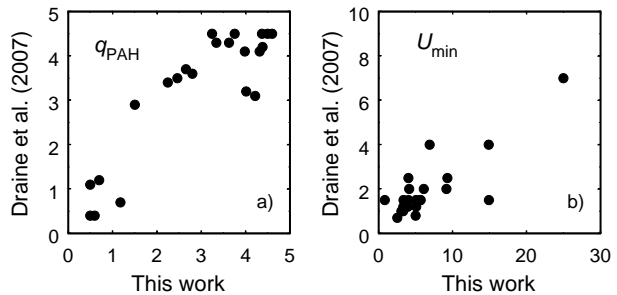


Figure 2. Comparison of q_{PAH} (a) and U_{min} (b) values obtained in this work and in Draine et al. (2007).

grain size distributions from Weingartner & Draine (2001), and they provide parameters for distributions only for dust mixtures in this range of q_{PAH} . Thus, we are unable to measure q_{PAH} values lower than 0.5% and greater than 4.6%. Note that q_{PAH} is insensitive to the band-to-band variations which can be caused by changes in the mean ionization state or grain size distribution.

4.1 Derived parameters of HII complexes

We have determined mass fraction of PAHs in more than 200 HII complexes for which metallicities are known. The combined results are presented in Fig. 3 both for the KK04 metallicity calibration and for the PT05 metallicity calibration. The metallicity threshold inferred in previous studies (Engelbracht et al. 2005; Draine et al. 2007; Gordon et al. 2008), which divides HII complexes with high and low PAH abundances, is apparently present in Fig. 3. It is ~ 8.4 in the KK04 scale and ~ 8.0 in the PT05 scale which is consistent with previous estimates. Depending on the method of metallicity estimation some previous studies quoted different values of the threshold. E. g., Draine et al. (2007), using the PT05 method, found the threshold to be ~ 8.1 , while Engelbracht et al. (2005) give the threshold value of about 8.2, using empirical methods that are close to the PT05 one.

When the KK04 calibration is used, a tendency is seen for the abundance of PAHs to grow with metallicity above the threshold (Fig. 3a). For the PT05 calibration there is more scatter on the q_{PAH} -metallicity plot that has a staggered appearance (Fig. 3b). As this scatter would blur any correlations that may exist in individual HII complexes, for the remainder of the present work, we adopt the KK04 metallicities. It must be kept in mind, however, that our conclusions are based on the specific metallicity calibration.

In Fig. 4, we show the metallicity vs. the PAH mass fraction q_{PAH} for several individual galaxies. In each subplot, we show the values for the entire sample (over all galaxies) as grey points, and the values for each individual galaxy (indicated by the caption) as black triangles.

We have only a few low-metallicity HII complexes in our sample, partly because these complexes are too faint in the infrared range. Furthermore, the SINGS/KINGFISH sample includes only four low-metallicity galaxies, and none of the HII complexes in these galaxies cover the ‘‘critical’’ metallicity range from about 8.2 to 8.5 (in the KK04 scale), which apparently includes the turn-off point. However, at higher metallicities, the tendency for the PAH content to grow with

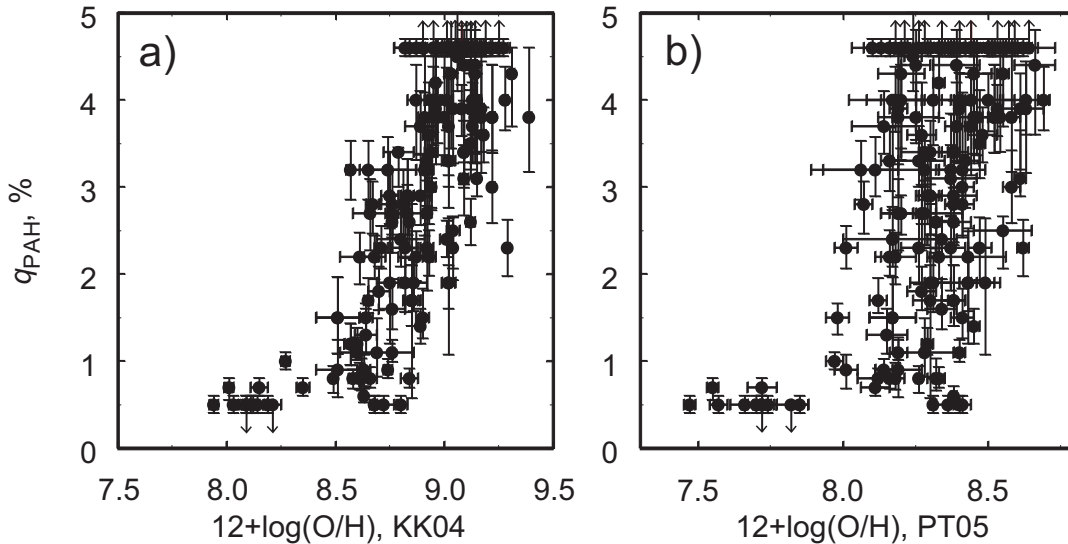


Figure 3. Relation between q_{PAH} and metallicity for individual HII complexes in all studied galaxies for the two metallicity calibrations.

$12 + \log(\text{O}/\text{H})$ is preserved, even when we consider individual HII complexes instead of an entire galaxy. This can be seen in Fig. 4, where we show data for selected galaxies from our sample with metallicities above the “critical” range. Despite the small number of data points for each galaxy, we still believe that our data are sufficient to conclude that the dependence of PAH content on the metallicity in star-forming galaxies is observed both globally and locally, at the scale of individual HII complexes. This result is consistent with the similar conclusion made by Gordon et al. (2008) for M101 galaxy.

In Fig. 5a we show how the PAH mass fraction q_{PAH} is related to the UV strength U_{min} . Solid circles correspond to HII complexes with q_{PAH} less than 4.6%, which is the highest value we can measure with our method. Open circles are HII complexes where the plotted q_{PAH} values represent lower limits. complexes with higher U_{min} tend to have lower q_{PAH} , albeit with significant scatter. The only noticeable exception is the CCM91 region in M51, which has a lower limit for q_{PAH} of 4.6%, and $U_{\text{min}} = 21$. It is interesting that high U_{min} values do indeed show some preference toward lower metallicity HII complexes (Fig. 5b). The apparent grouping of points in the lower part of Figure 5b simply reflects the lack of observed complexes and galaxies in the “critical” metallicity range. Probably, these intermediate systems are too faint in the infrared to become a part of some large-scale survey, but at the same time too metal-rich to deserve an individual study.

4.2 Dust indices, PAH content, and metallicity

Apart from the SED modelling, some indices can be used to characterize the dust content. Draine & Li (2007) introduced the $P_{8.0}$ and P_{24} indices

$$P_{8.0} = \frac{\nu F_{\nu}^{\text{ns}}(8.0\mu\text{m})}{\nu F_{\nu}(70\mu\text{m}) + \nu F_{\nu}(160\mu\text{m})}, \quad (4)$$

$$P_{24} = \frac{\nu F_{\nu}^{\text{ns}}(24\mu\text{m})}{\nu F_{\nu}(70\mu\text{m}) + \nu F_{\nu}(160\mu\text{m})}, \quad (5)$$

where $F_{\nu}^{\text{ns}}(8.0\mu\text{m})$ and $F_{\nu}^{\text{ns}}(24\mu\text{m})$ are non-stellar fluxes at 8 and 24 μm , correspondingly. Stellar emission significantly affects Spitzer 3.6 μm band; at 8 μm and 24 μm , the stellar contribution is less important, but still should be taken into account. We use the relations, given by Helou et al. (2004), to subtract stellar emission. At 70 and 160 μm , the stellar contribution is negligible, and no correction is applied to $F_{\nu}(70\mu\text{m})$ and $F_{\nu}(160\mu\text{m})$ fluxes.

Muñoz-Mateos et al. (2009) proposed an analytical relation (their Eq. A4) between q_{PAH} , $P_{8.0}$ and P_{24} , which allows estimation of the PAH content in cases when q_{PAH} goes beyond the limits of the Draine & Li (2007) spectra. In our data, the dependence of q_{PAH} on infrared indices look similar, but our q_{PAH} values are systematically lower than those computed for the same $P_{8.0}$ and P_{24} values with the analytical relation of Muñoz-Mateos et al. (2009). This is, probably, again related to the fact that we only consider HII complexes with enhanced UV radiation. In these complexes fewer PAHs are needed to produce a certain level of 8 μm emission compared to cases when this emission is averaged over the galaxy as a whole (or over a significant portion of the galaxy).

We considered several relations between metallicity and the $P_{8.0}$ and P_{24} indices. In Fig. 6, we show how $P_{8.0}$ and P_{24} are related to the metallicity of an HII complex. $P_{8.0}$ shows nearly the same correlation with metallicity as q_{PAH} (Fig. 6a). On the other hand, P_{24} appears to be totally uncorrelated with metallicity (Fig. 6b).

Naturally, $P_{8.0}$ is correlated with q_{PAH} as well (Fig. 7a), but this index, unlike q_{PAH} , is not bound to the model grid, so we used it to mark some q_{PAH} values as lower and upper limits. Specifically, we estimated the bordering values $P_{8.0}^{\text{min}}$ and $P_{8.0}^{\text{max}}$ that correspond to q_{PAH} of 0.5% and 4.6%, respectively. If $P_{8.0}$ for an HII region is greater than $P_{8.0}^{\text{max}}$ or less than $P_{8.0}^{\text{min}}$ we assume that the corresponding q_{PAH} value is an upper or lower limit.

The absence of correlation between P_{24} and metallicity implies that qualitative assessment of the PAH content in HII complexes can be done, using the $P_{8.0}/P_{24}$ ratio or, equivalently, the $F_{8.0}^{\text{ns}}/F_{24}^{\text{ns}}$ ratio. This ratio is sometimes con-

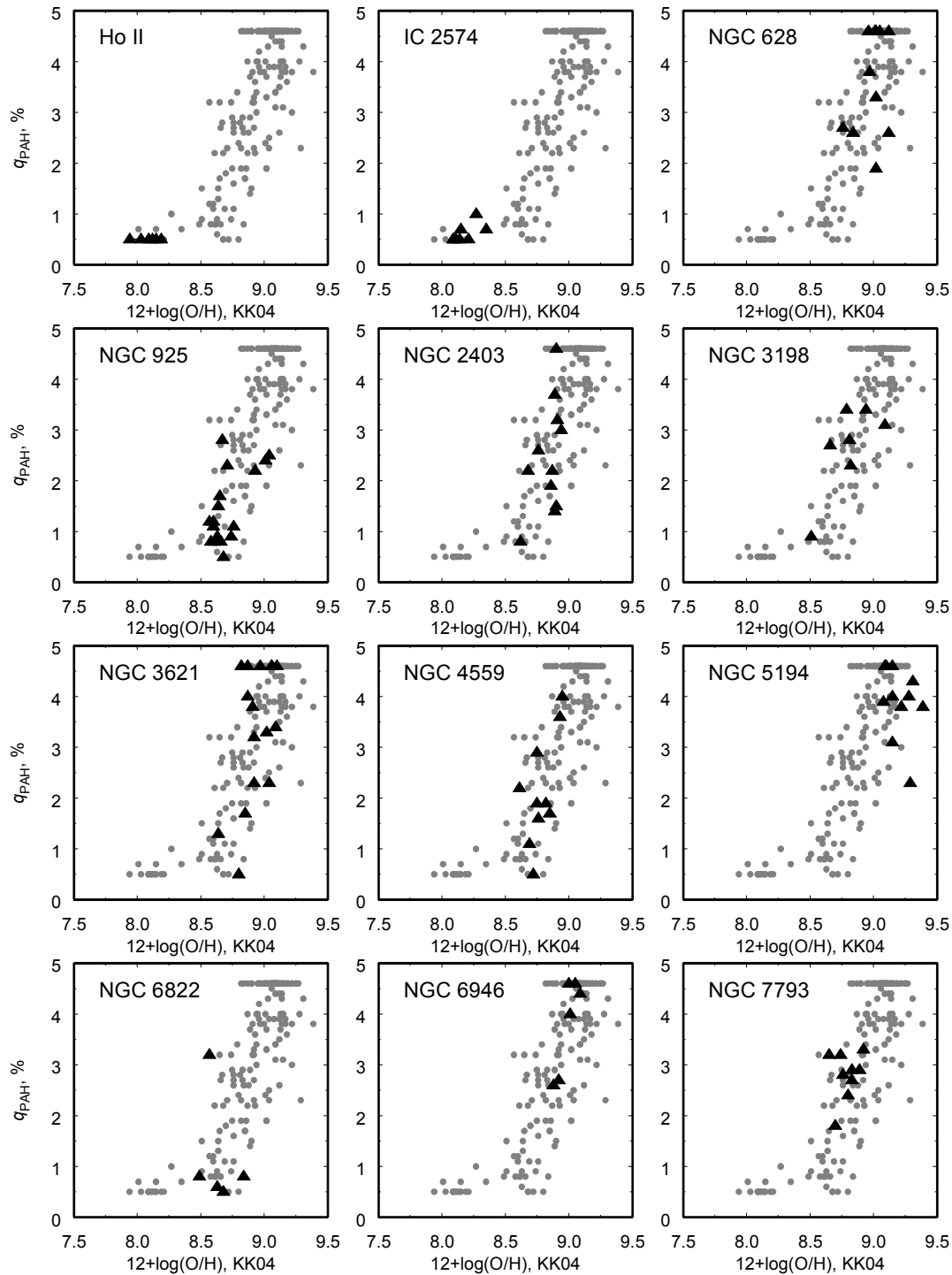


Figure 4. Relation between q_{PAH} and metallicity for individual HII complexes in selected galaxies. The grey points in each subplot show the values from the entire sample, while the triangles show only those values corresponding the galaxy indicated in the upper left. Galaxies which are not included in this plot have high metallicities so that the corresponding points are concentrated in the upper right part of the plot.

sidered to be a quantitative measure of the PAH abundance (Engelbracht et al. 2005). In our results, it is indeed well correlated with q_{PAH} (Fig. 7b). This greatly expands the ability to quantify the PAH evolution in HII complexes, as the $F_{8.0}^{\text{ns}}/F_{24}^{\text{ns}}$ ratio does not require photometry at longer IR wavelengths.

5 DISCUSSION

Our results indicate that the correlation between the PAH abundance and metallicity may exist both globally (for entire galaxies) and locally (for individual star-forming complexes). Here, we examine how the local character of the

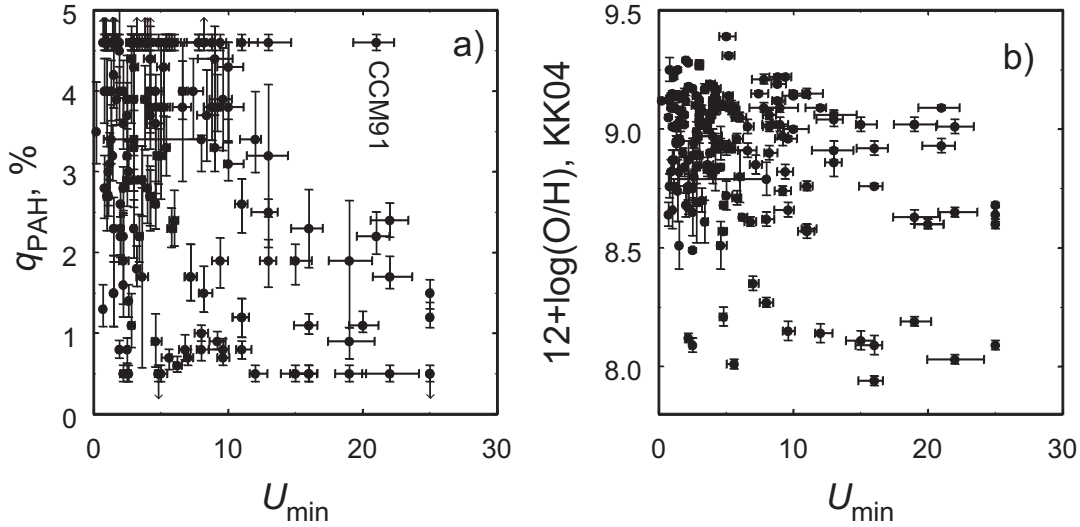


Figure 5. a) Relation between q_{PAH} and U_{min} values for all the studied HII complexes. b) Relation between the metallicity and U_{min} . Solid line shows the linear fit through all the data points.

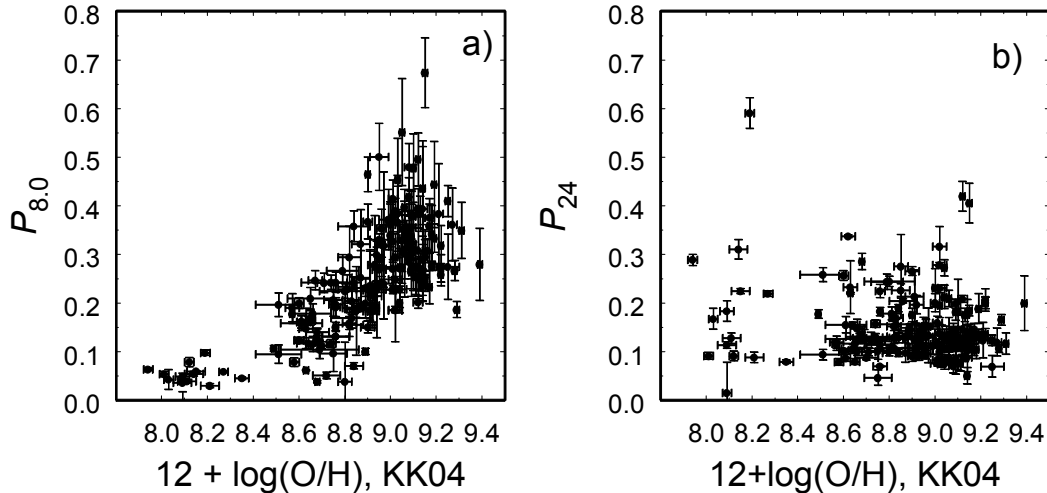


Figure 6. Relation between $P_{8.0}$ and P_{24} indices and the metallicity of an HII complex.

$q_{\text{PAH}} - (\text{O}/\text{H})$ correlation is related to our ability to understand the processes of PAH formation.

According to the “AGB” scenario, a low q_{PAH} value in low-metallicity environments reflects certain details of their synthesis in metal-poor AGB stars. Specifically, AGB stars populate low-metallicity galaxies as well as high-metallicity galaxies (Tosi 2009), but the carbon-to-oxygen ratio in the former may be too low for effective PAH formation.

Neither observational nor theoretical data currently seem to support this assertion unequivocally. There are indications that C/O ratio in the interstellar medium is roughly constant at metallicities lower than $12 + \log(\text{O}/\text{H}) \approx 8.0$ (at the direct method scale) and grows with (O/H) at higher metallicities (Henry et al. 2000). This behaviour is reminiscent of the observed PAH behaviour, and it is tempting to assume that the correlation between q_{PAH} and (O/H) simply reflects the correlation between C/O and (O/H).

However, a significant number of extremely metal-poor

stars with carbon overabundance implies that dependence of the C/O ratio on metallicity is more complicated than just “constant, then growing.” Also, there is still no direct observational evidence that PAHs are formed in the atmospheres of AGB stars, even though PAHs are observed in vicinities of some post-AGB and AGB stars with hot companions.

Circumstantial evidence is more difficult to interpret, as there are at least two additional factors that make the situation confusing. First, observations indicate that acetylene molecules, believed to be precursors for PAHs, are more abundant in low-metallicity AGB stars (Woods et al. 2012, and references therein). Woods et al. (2012) have shown with chemical modelling that these molecules, and other hydrocarbons, form more efficiently in the atmospheres of metal-poor stars compared to stars of solar metallicity. Second, metal-poor stars not only produce abundant complex hydrocarbons, but may also expel them into circumstellar space more efficiently (Mattsson et al. 2008). Also, from a

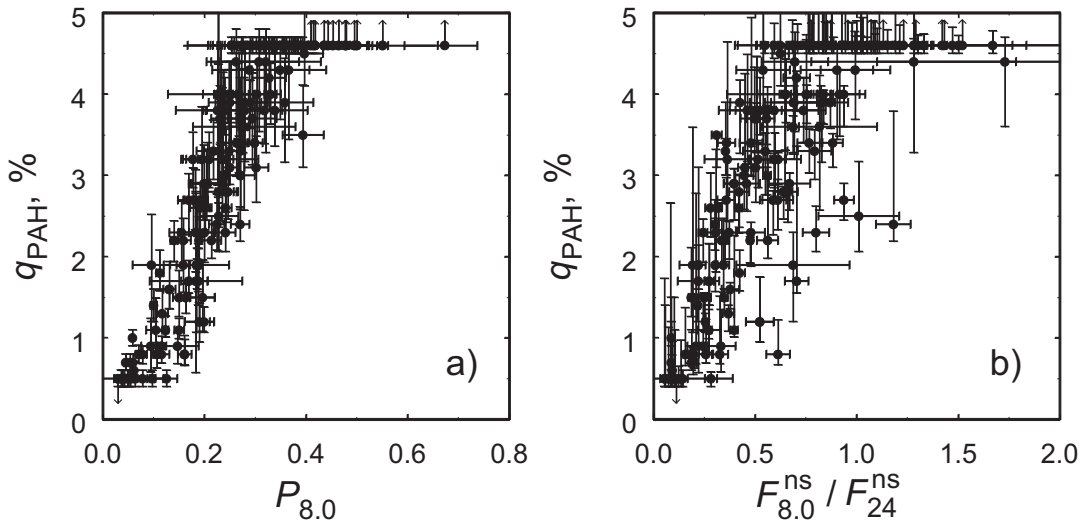


Figure 7. Relation between $P_{8.0}$ index, $F_{8.0}^{ns}/F_{24}^{ns}$ ratio, and the PAH content for individual HII complexes.

more general point of view, the evolution of C and O in AGB stars is defined by many processes that involve both synthesis and destruction, so that surface C/O ratio (supposedly related to PAH synthesis) depends not only on the star initial metallicity and mass, but also on time within the AGB phase (e.g., Lattanzio & Forestini 1999; Herwig 2005). So, it is well expected that initial metallicity would not play a simple role in determining the PAH synthesis. At the very least, low metallicity by itself does not guarantee fewer PAHs.

Another complication is the non-uniform and (possibly) time-dependent metallicity distribution in most late-type galaxies. If PAHs are synthesized in AGB stars with an efficiency that is an increasing function of metallicity, then the PAH content should depend on the metallicity of these parent stars (i.e., on the metallicity at locations where these stars were formed). The original relation between the PAH content and metallicity would be preserved if PAHs and/or their parent stars are not able to travel in the galaxy over significant distances (i.e., distances, over which the metallicity changes appreciably).

The question is if AGB stars can migrate over kiloparsec scales in their parent galaxies. Calculations show that radial mixing of stars can flatten the metallicity gradient both in the Milky Way-type galaxies, and in less-massive galaxies, over a time span comparable to the lifetime (from about 100 Myr to several Gyr) of an AGB star (Sellwood & Binney 2002; Minchev et al. 2011). The metallicity range in the galaxies from our sample does not exceed a few tenths. To destroy the original correlation between the PAH content and the ISM metallicity, the star would have to have moved radially by a few kiloparsecs prior to the AGB phase, which seems probable according to theoretical models. If this were the case, we would expect the metallicity gradient of evolved stars to be shallower than the gradient of the ISM metallicity, or the gradient measured with young objects like O stars or open clusters.

Observational evidence of this is not clear. According to some studies, both in our galaxy and in others, the metallicity gradient measured using planetary neb-

ulae (PN) is indeed the same (or even steeper) than the gradient measured with open clusters or HII regions (Maciel et al. 2005; Stanghellini et al. 2010; Magrini et al. 2009; Hernández-Martínez et al. 2009). According to other studies, however, the PN metallicity gradient is shallower than that of HII regions (Perinotto & Morbidelli 2006). Yu et al. (2012) found that the gradient steepens with the effective temperature of stars that have been used to measure the gradient. This again indicates that the gradient becomes shallower when we consider older objects, because of radial migration.

Thus, to have the PAH content correlated with the local ISM metallicity in the “AGB” scenario, we need three conditions to be satisfied. First, the efficiency of the PAH synthesis should be related to the metallicity of the parent AGB star. Second, the parent AGB star should stay in approximately the same metallicity environment during its lifetime. Third, PAHs should not leave this environment due to radial gas flows. Note that azimuthal mixing may also be important in this respect, as at least in the Milky Way there are some azimuthal metallicity variations (Balsler et al. 2011).

There is one more argument which may turn out to be contradictory to the “AGB” scenario. Supposing that VSGs are represented by PAH clusters, it is reasonable to assume that their formation processes are similar to those of PAHs. Thus, we may expect a correlation between P_{24} and metallicity, similar to what we see between $P_{8.0}$ and metallicity. However, there are no signs for such correlation (Fig. 6b).

This argument can be irrelevant if at some circumstances large grains over-power very small grains at 24 μ m. However, most studies where distinction is made between grains of various types indicate that in the general ISM most significant contribution at 24 μ m comes from VSGs (Desert et al. 1990; Compiègne et al. 2011). The same seems to be true in PDRs as well (Bernè et al. 2007; Compiègne et al. 2008). In the immediate vicinity of HII regions the situation is more complicated. Flagey et al. (2011) have shown that under certain assumption on the grain size distributions in some regions within the Eagle Nebula emis-

sion from big grains (BG) is indeed comparable or even exceeds emission from VSGs. Deharveng et al. (2010) analysed emission maps of several HII regions at 8 and 24 μm and stated that the source of emission at 24 μm (BGs vs VSGs) cannot be indentified clearly. We have initiated our own modelling of the infrared emission from an HII region that takes into account grain destruction and found that the contribution from big grains at 24 μm is small in comparison to the VSG contribution (M. Kirsanova et al., submitted). Still, the question of the 24 μm emission source is far from being solved.

In the “destructive” scenario, there is only one condition that needs to be met. Namely, the PAH destruction efficiency should be related to the local metallicity, i.e., through the intensity and/or hardness of the UV field. The relation between q_{PAH} and the UV intensity (characterized by U_{min}) does seem to exist, albeit with significant scatter (Fig. 5a). Regarding on the scatter in the $q_{\text{PAH}} - (\text{O}/\text{H})$ and $q_{\text{PAH}} - U_{\text{min}}$ relation, we must note that there are two unknowns in the “destructive” scenario that are able to smear out metallicity trends. These are the age of the HII region, and the initial PAH content q_{PAH}^0 , prior to the onset of star formation in the region.

The absence of the P_{24} correlation with (O/H) (Fig. 6) does not conflict with the “destructive” scenario (if the emission at 24 μm is indeed dominated by hot, small grains). It can be explained by the greater stability of small grains against the ultraviolet radiation field, compared to PAHs.

Some arguments in favour of the “destructive” scenario are presented in the spatially resolved mid-IR study of the Small Magellanic Cloud (SMC) by Bolatto et al. (2007) and Sandstrom et al. (2010). These authors have found a large range of the $F_{8.0}/F_{24}$ values across the SMC star-forming regions despite their relatively uniform metallicity and concluded that the metallicity-dependent formation cannot be the primary factor, determining the PAH abundance in the SMC. Sandstrom et al. (2010) also found that the $F_{8.0}/F_{24}$ ratio correlates with q_{PAH} , albeit with significant scatter. In our study the correlation appears to be stronger, but we only consider star-forming complexes, while in the SMC the greatest scatter in $F_{8.0}/F_{24}$ is apparently observed in the diffuse medium with $q_{\text{PAH}} < 1.5\%$ (Sandstrom et al. 2010).

The factors which determine the initial PAH content in an HII region are very diverse. First, the initial PAH molecules in a molecular cloud may be provided by AGB stars. In this case, the possible pre-existing $q_{\text{PAH}} - (\text{O}/\text{H})$ correlation, established globally due to metallicity-dependent PAH formation, can be further enhanced locally due to metallicity-dependent PAH destruction. Second, even if PAHs synthesized in AGB stars are completely destroyed as they travel through the intercloud space ($q_{\text{PAH}}^0 = 0$), they may be synthesized in molecular clouds. As far as we know, there are no studies that address the formation of PAHs in molecular clouds directly. However, there are other related studies, like Bettens & Herbst (1997). If PAHs are indeed able to form in molecular clouds, their observed content is determined by the balance between the local formation (possibly metallicity-dependent) and the local (metallicity-dependent) destruction. Third, PAHs observed in star-forming regions may represent an intermediate stage in the metallicity-dependent destruction of larger particles

(e.g., graphitic very small grains or amorphous hydrocarbon conglomerations).

To clarify the relative importance of all these factors, a detailed numerical model is needed (D. Wiebe et al., in preparation). Also, it would be useful to find a way to estimate the VSG mass fraction in HII complexes, and to explore whether or not it shows similar correlations as the PAH mass fraction.

6 SUMMARY AND CONCLUSIONS

In this work we performed aperture photometry for more than 200 HII complexes in 24 spatially-resolved nearby galaxies from the SINGS sample. Spitzer and Herschel data are used to estimate the PAH abundances and the UV field intensity in these HII complexes. Using literature values of the metallicities of the HII complexes, we show that the well-known correlation between the PAH content and metallicity previously found for entire galaxies is preserved also for smaller-structure components, like star-formation complexes and giant HII regions. We lack galaxies with $12 + (\text{O}/\text{H})$ around the threshold metallicity in our sample, so we are not able to trace the region in the $q_{\text{PAH}} - (\text{O}/\text{H})$ parameter space where q_{PAH} begins to increase with metallicity. Several arguments are presented in favour of the “destructive” scenario of PAH evolution, which relates the lower PAH mass fraction in low-metallicity environments to a stronger UV field. However, many factors are involved in PAHs evolution, so more detailed modelling should be able to provide more clear information on their evolutionary path.

ACKNOWLEDGMENTS

We are grateful to an anonymous referee for valuable comments and suggestions. This study was supported by the RFBR (grants 10-02-00231, 12-02-31452) and by the Federal Targeted Program “Scientific and Educational Human Resources of Innovation-Driven Russia” (contract with the Ministry of Science and Education 14.V37.21.0251). This work is based in part on observations made with the Spitzer Space Telescope, which is operated by the Jet Propulsion Laboratory, California Institute of Technology under a contract with NASA, and Herschel Space Observatory, which is an ESA facility with science instruments provided by European-led Principal Investigator consortia and with important participation from NASA. We thank Hendrik Linz for explanation of reduction process of Herschel data and essential help to this work, and Vitaly Akimkin for useful discussion.

REFERENCES

- Aniano, G., Draine, B. T., Gordon, K. D., Sandstrom, K. 2011, *PASP*, 123, 1218
- Arsenault, R., Roy, J.-R. 1986, *AJ*, 92, 567
- Balser, D. S., Rood, R. T., Bania, T. M., Anderson, L. D. 2011, *ApJ*, 738, id. 27
- Bendo, G. J., Draine, B. T., Engelbracht, C. W., et al. 2008, *MNRAS*, 389, 629

- Bernè, O., Joblin, C., Deville, Y., Smith, J. D., et al. 2007, *A&A*, 469, 575
- Bettens, R. P. A., Herbst, E. 1997, *ApJ*, 478, 585
- Bolatto, A. D., Simon, J. D., Stanimirović, S., van Loon, J. Th. et al. 2007, *ApJ*, 655, 212
- Boselli, A., Lequeux, J., Gavazzi, G. 2004, *A&A*, 428, 409
- Bresolin, F., Kennicutt, R. C., Garnett, D. R. 1999, *ApJ*, 510, 104
- Bresolin, F., Kennicutt, R. C. 2002, *ApJ*, 572, 838
- Bresolin, F., Garnett, D. R., Kennicutt, R. C. 2004, *ApJ*, 615, 228
- Calzetti, D., Kennicutt, R. C., Engelbracht, C. W., Leitherer, C., et al. 2007, *ApJ*, 666, 870
- Compiègne, M., Abergel, A., Verstraete, L., Habart, E. 2008, *A&A*, 491, 797
- Compiègne, M., Verstraete, L., Jones, A., Bernard, J.-P., et al. 2011, *A&A*, 525, id.A103
- Crocker, A. F., Calzetti, D., Thilker, D. A., Aniano, G., et al. 2013, *ApJ*, 762, 79
- Croxall, K. V., van Zee, L., Lee, H., Skillman, E. D., Lee, J. C., Côté, S., Kennicutt, R. C., Miller, B. W. 2009, *ApJ*, 705, 723
- Deharveng, L., Schuller, F., Anderson, L. D., Zavagno, A., Wyrowski, F., Menten, K. M., Bronfman, L., Testi, L., Walmsley, C. M., and Wienen, M. 2010, *A&A*, 523, A6
- Desert, F.-X., Boulanger, F., Puget, J. L. 1990, *A&A*, 237, 215
- Diaz, A. I., Terlevich, E., Vilchez, J. M., Pagel, B. E. J., Edmunds, M. G. 1991, *MNRAS*, 253, 245
- Draine, B. T., Dale, D. A., Bendo, G., Gordon, K. D. et al. 2007, *ApJ*, 663, 866
- Draine, B. T., Li, A. 2001, *ApJ*, 551, 807
- Draine B. T., Li A., 2007, *ApJ*, 657, 810
- Edmunds, M. G., Pagel, B. E. J. 1984, *MNRAS*, 211, 507
- Egorov, O., Lozinskaya, T. A., Moiseev, A. V. 2012, arXiv:1211.3969
- Engelbracht, C. W., Gordon, K. D., Rieke, G. H., Werner, M. W., Dale, D. A., Latter, W. B. 2005, *ApJ*, 628, 29
- Ferguson, A. M. N., Gallagher, J. S., Wyse, R. F. G. 1998, *AJ*, 116, 673
- Flagey, N., Boulanger, F., Noriega-Crespo, A., Paladini, R., Montmerle, T., Carey, S. J., Gagnè, M., Shenoy, S. 2011, *A&A*, 531, id.A51
- Galliano, F., Madden, S. C., Jones, A. P., Wilson, C. D., Bernard, J.-P. 2005, *A&A*, 434, 867
- Galliano, F., Dwek, E., Chaniai, P. 2008, *ApJ*, 672, 214
- Garnett, D. R., Shields, G. A., Skillman, E. D., Sagan, S. P., Dufour, R. J. 1997, *ApJ*, 489, 63
- Garnett, D. R., Shields, G. A., Peimbert, M., Torres-Peimbert, S., Skillman, E. D., Dufour, R. J., Terlevich, E., Terlevich, R. J. 1999, *ApJ*, 513, 168
- Gordon, K. D., Engelbracht, Ch. W., Rieke, G. H., Misselt, K. A., Smith, J.-D. T., Kennicutt, R. C. Jr. 2008, *ApJ*, 682, 336
- Haynes, K., Cannon, J. M., Skillman, E. D., Jackson, D. C., Gehr, R. 2010, *ApJ*, 724, 215
- Helou, G., Roussel, H., Appleton, P., Frayer, D. et al. 2004, *ApJS*, 154, 253
- Henry, R. B. C., Pagel, B. E. J., Chincarini, G. L. 1994, *MNRAS*, 266, 421
- Henry, R. B. C., Edmunds, M. G., Köppen, J. 2000, *ApJ*, 541, 660
- Hernández-Martínez, L., Pena, M., Carigi, L., García-Rojas, J. 2009, *A&A*, 505, 1027
- Herwig, F. 2005, *ARA&A*, 43, 435
- Hodge, P., Lee, M. G., Kennicutt, Jr., R. C. 1988, *PASP*, 100, 917
- Hodge, P., Strobel, N. V., Kennicutt, R. C. 1994, *PASP*, 106, 309
- Hunt, L. K., Thuan, T. X., Izotov, Y. I., Sauvage, M. 2010, *ApJ*, 712, 164
- Kennicutt, R. C., Armus, L., Bendo, G., Calzetti, D. et al. 2003, *PASP*, 115, 928
- Kennicutt, R. C., Hao, C.-N., Calzetti, D., et al., 2009, *ApJ*, 703, 1672
- Kennicutt, R. C., Calzetti, D., Aniano, G., et al. 2011, *PASP*, 123, 1347
- Kim, J. H., Im, M., Lee, H. M., Lee, M. G., et al. 2012, *ApJ*, 760, 120
- Kobulnicky, H. A., Kewley, L. J. 2004, *ApJ*, 617, 240
- Lattanzio, J., Forestini, M. 1999, Asymptotic giant branch stars, Proceedings of the IAU symposium 191. Eds T. Le Bertre, A. Lebre, & C. Waelkens. Astronomical Society of the Pacific: California, USA , 1999, p. 31
- Latter, W. B. 1991, *ApJ*, 377, 187
- Lee, H., Skillman, E. D. 2004, *ApJ*, 614, 698
- Lee, H., Skillman, E. D., Venn, K. A. 2006, *ApJ*, 642, 813
- Li A., Draine, B. T. 2002, *ApJ*, 572, 232
- Lopez-Sanchez, A. R., Dopita, M. A., Kewley, L. J., Zahid, H. J., Nicholls, D. C., Scharwachter, J. 2012, *MNRAS*, in press, astro-ph/1203.5021
- Maciel, W. J., Lago, L. G., Costa, R. D. D. 2005, 433, 127
- Madden S. C., Galliano, F., Jones, A. P., Sauvage, M. 2006, *A&A*, 446, 877
- Magrini, L., Stanghellini, L., Villaver, E. 2009, *ApJ*, 696, 729
- Mathis J. S., Mezger, P. G., Panagia, N. 1983, *A&A*, 128, 212
- Mattsson, L., Wahlin, R., Höfner, S., Eriksson, K. 2008, *A&A*, 484, L5
- McCall, M. L., Rybski, P. M., Shields, G. A. 1985, *ApJS*, 57, 1
- Minchev, I., Famaey, B., Combes, F., Di Matteo, P., Mouhcine, M., Wozniak, H. 2011, *A&A*, 527, A147
- Moustakas, J., Kennicutt, R. C., Tremonti, C. A., Dale, D. A., Smith, J. -D. T., Calzetti, D. 2010, *ApJS*, 190, 233
- Muñoz-Mateos, J. C., Gil de Paz, A., Boissier, S., Zamorano, J. et al. 2009, *ApJ*, 701, 1965
- Oey, M. S., Kennicutt, R. C. 1993, *ApJ*, 411, 137
- O'Halloran, B., Satyapal, S., Dudik, R. P. 2006, *ApJ*, 641, 795
- Pavlyuchenkov, Ya. N., Wiebe, D. S., Akimkin, V. V., Khrantsova, M. S., Henning, Th., 2012, *MNRAS*, 421, 2430
- Perinotto, M., Morbidelli, L. 2006, *MNRAS*, 372, 45
- Pilyugin, L. S., Thuan, T. X. 2005, *ApJ*, 631, 231
- Poglitsch, A., Waelkens, C., Geis, N., Feuchtgruber, H., Vandenbussche, B., Rodriguez, L., Krause, O., et al. 2010, *A&A*, 218, 2P
- Roussel, H., 2012, submitted to *PASP*
- Ryder, S. D. 1995, *ApJ*, 444, 610
- Sandstrom, K. M., Bolatto, A. D., Draine, B. T., Bot, C., Stanimirović S. 2010, 715, 701
- Sellwood, J. A., Binney, J. J. 2002, *MNRAS*, 336, 785

- Shields, G. A. 1991, *PASP*, 103, 916
- Slater, C. T., Oey, M. S., Li, A., Bernard, J.-P., et al. 2011, *ApJ*, 732, 98
- Smith, J. D. T., Draine, B. T., Dale, D. A., Moustakas, J. et al. 2007, *ApJ*, 656, 770
- Stasińska, G. 2007, in *Canary Islands Winter School of Astrophysics*, CUP 2008, p. 1
- Stanghellini, L., Magrini, L., Villaver, E., Galli, D. 2010, *A&A*, 521, A3
- Tosi, M. 2009, *A&A*, 500, 157
- Treyer, M., Schiminovich, D., Johnson, B. D., O'Dowd, M., et al. 2010, *ApJ*, 719, 1191
- van Zee, L., Salzer, J. J., Haynes, M. P., O'Donoghue, A. A., & Balonek, T. J. 1998, *AJ*, 116, 2805
- Weingartner J. C., Draine B. T., 2001, *ApJ*, 548, 296
- Woods, P. M., Walsh, C., Cordiner, M. A., Kemper, F. 2012, *MNRAS*, in press
- Wu, H., Zhu, Y.-N., Cao, C., Qin, B. 2007, *ApJ*, 668, 87
- Yu, J., Sellwood, J. A., Pryor, C., Chen, L., Hou, J. 2012, *ApJ*, in press
- Zaritsky, D., Kennicutt, R. C., Huchra, J. P. 1994, *ApJ*, 420, 87
- Zhu, Y.-N., Wu, H., Cao, Ch., Li, H.-N. 2008, *ApJ*, 686, 155

Table 2: Parameters of HII complexes. Full table is available online.

No.Object		α (J2000) <i>h m s</i>	δ (J2000) <i>° ' "</i>	aperture radius, "	$F_{3.6}$, mJy	$F_{4.5}$, mJy	$F_{5.8}$, mJy	$F_{8.0}$, mJy	F_{24} , mJy	F_{70} , mJy	F_{160} , mJy
IC2574											
1	H1	10 28 55.60	+68 27 54.8	12.0	0.01 ± 0.01	0.01 ± 0.01	0.07 ± 0.01	0.15 ± 0.01	2.3 ± 0.1	3.6 ± 1.8	2.2 ± 2.0
2	H2	10 28 58.91	+68 28 27.7	14.0	0.12 ± 0.01	0.10 ± 0.01	0.21 ± 0.02	0.31 ± 0.01	2.7 ± 0.1	45.9 ± 2.4	55.1 ± 6.1
3	H3	10 28 48.50	+68 28 02.3	13.0	0.34 ± 0.03	0.36 ± 0.02	1.10 ± 0.03	2.4 ± 0.1	27.2 ± 0.3	259.4 ± 6.3	225.9 ± 8.5
4	H5-6	10 28 50.18	+68 28 23.3	14.0	0.19 ± 0.03	0.17 ± 0.02	0.33 ± 0.04	0.63 ± 0.07	5.3 ± 0.6	129.7 ± 6.6	111.3 ± 6.8
5	H8	10 28 43.65	+68 28 26.4	12.0	0.22 ± 0.04	0.29 ± 0.04	0.30 ± 0.04	0.51 ± 0.03	8.0 ± 0.2	60.7 ± 4.0	35.1 ± 4.7
6	H10	10 28 39.30	+68 28 06.9	12.0	0.16 ± 0.02	0.16 ± 0.02	0.19 ± 0.01	0.31 ± 0.01	2.7 ± 0.2	44.5 ± 3.6	43.2 ± 3.4
7	H13-14	10 28 30.84	+68 28 08.4	12.0	0.06 ± 0.01	0.04 ± 0.01	0.08 ± 0.01	0.09 ± 0.01	0.8 ± 0.1	8.7 ± 0.8	11.3 ± 2.8
8	II	10 28 48.40	+68 28 02.0	14.0	0.35 ± 0.03	0.36 ± 0.02	1.10 ± 0.03	2.5 ± 0.1	28.0 ± 0.3	273.1 ± 7.2	236.7 ± 9.2
9	III	10 28 50.91	+68 25 26.1	14.0	0.34 ± 0.02	0.30 ± 0.01	0.52 ± 0.24	0.84 ± 0.03	4.1 ± 0.2	104.2 ± 2.9	112.1 ± 4.2

Table 3: Fitting parameters of HII complexes and metallicities. Full table is available online.

No.Object	q_{PAH}	$\gamma, \%$	U_{min}	$12 + \log(\text{O}/\text{H})$ KK04	$12 + \log(\text{O}/\text{H})$ PT05	
IC2574						
1	H1	$0.5^{+0.1}_{-0.1}$	$30.0^{+0.1}_{-0.1}$	$7.6^{+0.5}_{-0.6}$	8.14 ± 0.04	7.71 ± 0.05
2	H2	$0.5^{+0.1}_{-0.1}$	$1.3^{+0.1}_{-0.1}$	$16.0^{+0.6}_{-1.4}$	8.09 ± 0.04	7.72 ± 0.05
3	H3	$0.7^{+0.1}_{-0.1}$	$4.5^{+0.1}_{-0.1}$	$9.6^{+0.5}_{-0.4}$	8.15 ± 0.04	7.72 ± 0.05
4	H5-6	$0.5^{+0.1}_{-0.1}$	$1.3^{+0.1}_{-0.2}$	$4.8^{+0.2}_{-0.3}$	8.21 ± 0.04	7.82 ± 0.06
5	H8	$0.5^{+0.1}_{-0.1}$	$8.4^{+0.2}_{-0.8}$	$12.0^{+0.9}_{-0.4}$	8.14 ± 0.04	7.72 ± 0.05
6	H10	$0.5^{+0.1}_{-0.1}$	$1.3^{+0.0}_{-0.1}$	$15.0^{+1.0}_{-1.1}$	8.11 ± 0.04	7.70 ± 0.05
7	H13-14	$0.5^{+0.1}_{-0.1}$	$4.5^{+0.1}_{-0.1}$	$2.5^{+0.1}_{-0.2}$	8.09 ± 0.03	7.66 ± 0.05
8	II	$1.0^{+0.1}_{-0.1}$	$4.5^{+0.1}_{-0.1}$	$8.0^{+0.5}_{-0.5}$	8.27 ± 0.02	7.97 ± 0.03
9	III	$0.7^{+0.1}_{-0.1}$	$1.3^{+0.1}_{-0.2}$	$7.0^{+0.4}_{-0.3}$	8.35 ± 0.03	8.11 ± 0.05